Battery Power Smoothing Control in a Marine Electric Power Plant using Nonlinear Model Predictive Control

Torstein Ingebrigtsen Bø, *Member, IEEE,* Tor Arne Johansen, *Member, IEEE,*

***Abstract*—This paper presents a power variation smoothing method using batteries on a weak ship grid. For some marine vessels, power fluctuations on the ac grid are large. This results in large variations in the electrical frequency of the grid and excessive wear and tear of the power producers. Adding batteries connected to a DC/AC drive to smooth out the power fluctuations has been suggested. However, due to the large amount of fluctuation, batteries can overheat. Therefore, we suggest using a band-pass filter with cutoff frequency parameters optimized by model predictive control based on a power spectral density estimate of power consumption for disturbance prediction.**

***Index Terms*—Battery management systems, Statistical analysis, Optimal control, Stochastic Model Predictive Control, Temperature control.**

I. Introduction

Marine vessels with diesel-electric power plants and propulsion have a weak ac grid, due to the large size of the consumers compared with the size and number of producers. Therefore, a typical load change will induce voltage and frequency variations. On some marine vessels, the power consumption fluctuates heavily in certain operational and environmental conditions. Due to the weak grid, this induces fluctuations in electrical frequency, excessive wear and tear on the power producers, and synchronization problems when connecting a new generator set to the grid. Currently, this problem is solved by connecting additional generators, which gives a stiffer grid. This reduces the efficiency of the plant and increases the need for maintenance.

The power fluctuations on a vessel may come from heave-compensators, auxiliary systems, wave-induced thruster disturbance, rapid changing thrust losses due to ventilation and thruster-thruster interaction, and hotel loads. The period typically varies from 0.1 seconds to hundreds of seconds. Diesel engines prefer to have as constant a load as possible, since this reduces thermal stress due to temperature changes. In the authors experience, diesel engines are not able to compensate for loads with dynamics faster than about 5-10 seconds due to the turbo-lag. On the other hand, the inertia of the generator set can compensate for some load fluctuations. Typically, the inertia can handle dynamics faster than 1-3 seconds. However, this increases the mechanical stress on the generator set. On a marine vessel, the total produced power can be measured at the generators. This is often done every 0.1 second. Therefore, a power smoothing algorithm should be able to handle fluctuations with periods from 0.1 to 100 seconds, but particularly where it is most important to take care of loads fluctuations i.e., periods between 1 and 10 seconds.

Several methods to reduce power fluctuations on marine vessels have already been proposed. Using the thruster allocation and feedforward in the governor to reduce power fluctuations has been proposed in [1], [2]. Another approach was to use the thrusters directly for power smoothing by generating a thruster load which counteracts other load variations [3], [4]. Typically, thruster biasing is used on vessels with dynamic positioning systems to reduce load variations; thrusters counteract each other to waste power, so that other load variations are canceled out [5].

Recently, adding batteries to the grid has been suggested. M/S Viking Queen will soon be retrofitted with batteries [6], while M/S Ampere is in operation and is driven by batteries only [7]. Using batteries on naval vessels to take care of pulse loads from the weapons system has been suggested [8], [9]. Batteries can also be used for emergency power, as demonstrated in [10]. In this article, batteries are used for power smoothing. Batteries compensate for the variations in power consumption, while the generator sets produce slowly varying power to meet the demand. The batteries used for this task must be able to charge and discharge large currents. However, since the mean current is zero, the storage capacity can be small. One problem with such a large charge and discharge current is that this produces heat. This heat production must be controlled or the batteries may disconnect due to overheating. On some vessels, batteries can be used for emergency power, this requires a larger battery, which is less prone to heat challenges. Battery power smoothing has already been proposed in [11], [12], [13].

The battery should remove as much power of the variation as possible. However, the battery can get hot if all variations are canceled when the power variations are large. In such cases, only the most critical load variations should be removed. In other cases, the load variations may be small and the batteries are able to cancel all load variations without overheating. Therefore, a dynamic approach should be used so that

T.I. Bø and T.A. Johansen are with center for autonomous marine operations and systems (NTNU AMOS), Department of Engineering Cybernetics, NTNU - Norwegian University of Science and Technology, 7491, Trondheim, Norway (e-mail: torstein.bo@itk.ntnu.no).

The authors of this paper are funded by the project design to verification of control systems for safe and energy efficient vessels with hybrid power plants (D2V), where the Research Council of Norway is the main sponsor. NFR: 210670/070, 223254/F50.

This work was also partly supported by the Research Council of Norway through the Center of Excellence funding scheme, project number 223254 - NTNU AMOS

the power variations to be removed are chosen dynamically, depending on the power variations and the temperature of the battery. We therefore suggest a hierarchy of controllers, with a high-level controller selecting which periods of the load fluctuations to remove and a low-level controller that takes care of the power smoothing and only removes the periods given by the high-level controller.

The power smoothing problem has similarities to the *power split* problem in hybrid electric vehicles, where the desired torque is generated by a combustion engine and an electric motor with a battery. Different strategies have been suggested and for the original Toyota Prius a rule-based controller was used [14]. Stochastic model predictive control has been suggested [15], as well as using dynamic programming for the design of a rule-based controller [16]. A controller that minimize fuel consumption and emissions is presented in [17]. Battery energy storage systems (BESS) have also been proposed for wind turbine plants. BESS can be used to smooth power fluctuations due to wind speed variations [18], [19]. In [20], it is demonstrated how BESS can be used in an isolated power grid to reduce frequency variations.

Model predictive control (MPC) is used in this paper as the high-level controller. A model of the plant is used in the MPC to predict the future state of the system, and a cost function is used to evaluate the future performance of the system. The MPC optimizes the cost for the prediction horizon. At every step, the free variables are optimized with respect to the cost function and constraints, and only the variables for the first step are applied to the system. Multiple suggestions using MPC in marine power plants already exist, such as [1], [21], [22], [23].

We use probabilistic constraints in this paper, as future load prediction is uncertain. These are constraints of the form $\text{Prob}(X < x_{\min}) < \eta$, where $\text{Prob}(\cdot)$ is the probability, $0 < \eta \ll 1$ is the probability threshold, and X is a random variable. For a linear system with Gaussian disturbance, it has been shown that the constraints can be converted to an explicit second-order cone constraints [24]. The use of scenarios and conditional value at risk (cVaR) as an approximation to the probabilistic constraint has also been suggested [25]. In [26], an approximation of chance constraints using scenarios and mixed integer quadratic programming is presented.

The main contribution of this paper is a controller which can adaptively optimize parameters based on estimates of the consumer demand power spectral density. It is applied to the optimal tuning of *power smoothing*. This is done using batteries to smooth out variations in the power demands of a marine vessel. The battery is controlled by a band-pass filter, so that only power variations over a given frequency band are counteracted.

The paper is organized as follows: the control plant model is introduced in Sec. II. The chance constraints used in the MPC are introduced in Sec. III. Sec. IV presents the controller. A simulation study is shown in Sec. V, before conclusions are drawn in Sec. VI. An appendix with mathematical preliminaries is included at the end of the paper.

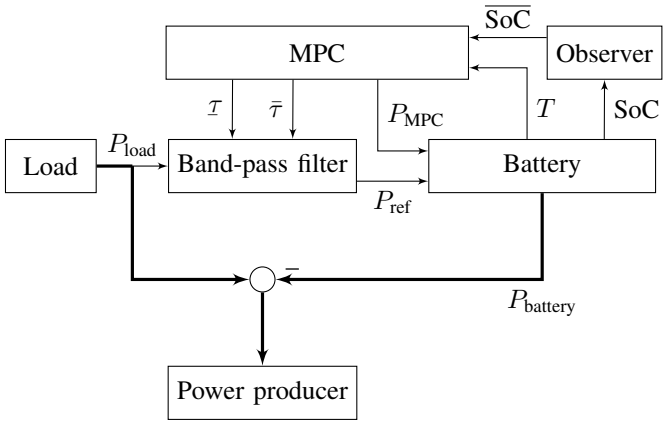

Fig. 1. Control hierarchy for power smoothing control. The thick lines represent electric power, while the thin lines represent control signals and measurements.

II. Control Plant

The control architecture is shown in Fig. 1. A load consumes the load P_{load}, which is random. A battery is used to smooth the fluctuations in the generated power. The goal is to keep the temperature and state of charge of the battery within operational limits, while reducing the power fluctuations in the generator set as much as possible.

The charging and discharging power of the battery is given by a band-pass filter. The input to the band-pass filter is P_{load}, while the output is the desired charging power, P_{ref}. This cancels out power fluctuations with frequencies between the cut-off frequencies of the band-pass filter. This gives a zero-mean charging power of the battery. However, the battery will still be discharged even with zero-mean charging power, due to ohmic losses and self-discharge. To avoid the battery discharging, the MPC calculates a mean charging power, P_{MPC}.

It should be noted that the measurements of generated power may not be synchronized and may have errors. In this study, we assume that the total consumed and generated power is measured without any error.

Heat generation due to high current through the battery must be limited to avoid it overheating. Therefore, the MPC adjusts the time constants of the band-pass filter to avoid too high battery temperatures.

A first-order high-pass filter and low-pass filter are put in series to implement a band-pass filter. However, any linear band-pass filter could have been chosen. The transfer function for this filter is:

$$H_f(j\omega) = \frac{P_{\text{ref}}(j\omega)}{P_{\text{load}}(j\omega)} = \frac{\bar{\tau} j\omega}{(1+\underline{\tau} j\omega)(1+\bar{\tau} j\omega) n_{\text{cells}}} \quad (1)$$

where $\bar{\tau}$ and $\underline{\tau}$ are the highest and lowest time constants of the band-pass filter, and n_{cells} is the number of cells in the battery. $\bar{\tau}$ and $\underline{\tau}$ are set by the MPC controller.

A simple model is used for the battery, as shown in Fig. 2. The internal resistance, R_i, and open circuit voltage, V_o, are

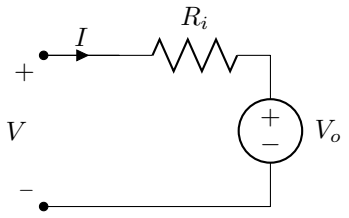

Fig. 2. Model of battery used internally in the MPC with internal resistance, R_i, and open circuit voltage, V_o, output voltage and current, V and I.

assumed to be constant. The temperature of the battery is modeled by Newton's law of cooling:

$$\frac{\mathrm{d}T}{\mathrm{d}t} = \frac{hA}{c}\left(T_{\text{air}} - T\right) + \frac{1}{c}Q_{\text{el}} \tag{2}$$

where T is the battery temperature, h is the heat transfer coefficient, A is the surface area of the battery, c is the heat capacity of the battery, T_{air} is the temperature of the cooling air, and Q_{el} is the heat generated in the battery. The heat is assumed to be equal to the electrical loss

$$Q_{\text{el}} = R_i I^2 \tag{3}$$

where R_i is the internal resistance of the battery, and I is the current through the battery.

Due to safety requirements the battery has a temperature limit for operation:

$$T \leq T_{\max}. \tag{4}$$

When this limit is reached, the battery must be disconnected until it has cooled down.

The charging power, P_{battery}, is controlled by a bi-directional AC/DC converter. It is set to the sum of the references from the band-pass filter and the mean charging power, P_{MPC}, calculated by the MPC:

$$P_{\text{battery}} = P_{\text{ref}} + P_{\text{MPC}}. \tag{5}$$

Setting $P_{\text{battery}} = I(V_o + R_i I)$, solving for the current, and using the Taylor expansion we get:

$$\begin{aligned} I &= \frac{-V_o + \sqrt{V_o^2 + 4R_i P_{\text{battery}}}}{2R_i} \\ &= \frac{P_{\text{battery}}}{V_o} - \frac{P_{\text{battery}}^2 R_i}{V_o^3} + O(P_{\text{battery}}^3) \end{aligned} \tag{6}$$

where $O(P_{\text{battery}}^3)$ denotes terms of order three or higher. The first- and second-order approximations will be used later, the higher order terms are assumed to be small.

The state of charge (SoC) of the battery is modeled as an integrator of the current [15]:

$$\frac{\mathrm{dSoC}}{\mathrm{d}t} = \frac{I}{Q_{\text{nominal}}} \tag{7}$$

where Q_{nominal} is the rated charge of the battery. Hence, the SoC of the battery is 0 when empty and 1 when fully charged. It is assumed that SoC is estimated by an external observer, as SoC estimates from Coulomb counting may drift-off. Multiple methods exist for such estimations, e.g., [27], [28], [29].

The battery may also be used for emergency power. We therefore assume a minimum state of charge constraint:

$$\mathrm{SoC}_{\min} \leq \mathrm{SoC} \leq \mathrm{SoC}_{\max}. \tag{8}$$

The minimum and maximum state of charge can be set by an operator or a plant optimizer. $\mathrm{SoC}_{\min}$ and $\mathrm{SoC}_{\max}$ can be used to avoid the ageing of the lithium batteries as this accelerates at low and high SoC.

However, since P_{Load} is stochastic we reformulate (8) to two probabilistic constraints:

$$\begin{aligned} \mathrm{Prob}(\mathrm{SoC}_{\min} \leq \mathrm{SoC}) &\geq 1 - \eta_{\mathrm{SoC}} \\ \mathrm{Prob}(\mathrm{SoC} \leq \mathrm{SoC}_{\max}) &\geq 1 - \eta_{\mathrm{SoC}} \end{aligned} \tag{9}$$

where η_{SoC} is the chosen probability threshold for violation of the constraint.

The temperature of the battery depends on P_{battery}. Since P_{battery} is random, T is also random. However, an estimate of the expected temperature is useful for the MPC. From (2):

$$\frac{\mathrm{d}}{\mathrm{d}t}E[T] = \frac{hA}{c}\left(T_{\text{air}} - E[T]\right) + \frac{1}{c}E[Q_{\text{el}}] \tag{10}$$

using the linear approximation of the current from (6) (neglecting second-order and higher terms), the expected heat loss is:

$$E\left[Q_{\text{el}}\right] \approx E\left[\frac{P_{\text{battery}}^2 R_i}{V_o^2}\right] \tag{11}$$

Note that $E\left[P_{\text{battery}}^2\right] = P_{\text{MPC}}^2 + \sigma_{p_{\text{ref}}}^2$, as $E[P_{\text{ref}}] = 0$ due to the band-pass filter and $\mathrm{var}\left[P_{\text{MPC}}\right] = 0$ (for one sample), this gives $E[P_{\text{MPC}}P_{\text{ref}}] = 0$ and

$$E\left[Q_{\text{el}}\right] \approx R_i \frac{P_{\text{MPC}}^2 + \sigma_{p_{\text{ref}}}^2}{V_o^2}. \tag{12}$$

The variance of P_{ref} can be estimated by (26) and (27)

$$\sigma_{p_{\text{ref}}}^2 = \int_0^\infty p_{pp}(\omega)|H_f(j\omega)|^2 \,\mathrm{d}\omega. \tag{13}$$

where $p_{pp}(\omega)$ is the power spectral density of P_{load}.

Note that the temperature variance will be small if the time constant of the temperature (c/hA) is large compared with the largest period in $p_{pp}(\omega)|H_f(j\omega)|^2$ with significant power. Constraining the expected value is therefore reasonable. Also note that $E[Q_{\text{el}}(t)]$ is not constant due to the dependency of the states of the linear filter. However, we assume that the filter time-constants are small compared with the time steps of the MPC. The temperature will therefore be close to the expected value estimated above.

III. Chance Constraint

An example of how to approximate chance constraints is given in this section. We need to convert the chance constraints (9) to explicit constraints. Assuming that P_{load} is close to a normal distribution and the nonlinearities of the SoC dynamics are small, SoC can be approximated to be normal distributed. Using (28), the chance constraints can be approximated to

$$\begin{aligned} \mathrm{SoC}_{\min} &\leq E[\mathrm{SoC}] - F^{-1}(1 - \eta_{\mathrm{SoC}})\sigma_{\mathrm{SoC}} \\ \mathrm{SoC}_{\max} &\geq E[\mathrm{SoC}] + F^{-1}(1 - \eta_{\mathrm{SoC}})\sigma_{\mathrm{SoC}} \end{aligned} \tag{14}$$

where $F^{-1}(\cdot)$ is the inverse cumulative distribution function of the standard normal distribution.

An estimate of $E[\text{SoC}]$ and σ^2_{SoC} is needed. By using the expected value of (7) and using the second-order approximation of (6):

$$\begin{aligned}\frac{\mathrm{d}}{\mathrm{d}t}E\left[\text{SoC}\right] &\approx E\left[\frac{P_{\text{battery}}}{V_o Q_{\text{nominal}}} - \frac{P^2_{\text{battery}} R_i}{V_o^3 Q_{\text{nominal}}}\right] \\ &= \frac{P_{\text{MPC}}}{V_o Q_{\text{nominal}}} - \frac{(P^2_{\text{MPC}} + \sigma^2_{p_{\text{ref}}}) R_i}{V_o^3 Q_{\text{nominal}}}. \end{aligned} \tag{15}$$

By linearizing (6), a linear system from P_{load} to SoC is found:

$$\frac{\text{SoC}(j\omega)}{P_{\text{load}}(j\omega)} = \frac{H_f(j\omega)}{Q_{\text{nominal}} V_o} \tag{16}$$

The variance of SoC can be estimated by (16), (26) and (27)

$$\sigma^2_{\text{SoC}} \approx \int_0^\infty p_{pp}(\omega) \frac{|H_f(j\omega)|^2}{Q^2_{\text{nominal}} V_o^2} \,\mathrm{d}\omega \tag{17}$$

The state of charge can be approximated as a slowly varying mean, $E[\text{SoC}]$, with a superimposed noise, v.

$$\text{SoC} = E[\text{SoC}] + v \tag{18}$$

where $E[\text{SoC}]$ is calculated by (15). To estimate $E[\text{SoC}]$ a discrete Kalman filter is applied, where SoC is the "measured state". The process is modeled as:

$$\frac{\mathrm{d}\overline{\text{SoC}}}{\mathrm{d}t} = \frac{P_{\text{MPC}}}{V_o Q_{\text{nominal}}} - \frac{(P^2_{\text{MPC}} + \sigma^2_{p_{\text{ref}}}) R_i}{V_o^3 Q_{\text{nominal}}} + w \tag{19}$$

$$y = \overline{\text{SoC}} + v \tag{20}$$

where $\overline{\text{SoC}}$ is the mean state of charge, $E[\text{SoC}]$; w is the "process noise", which should capture the model errors of $E[\text{SoC}]$ including linearization errors and self-discharge; and v is the "measurement noise", which is the current deviation of the state of charge from the mean state of charge. The noise v is approximated to be white noise with variance σ^2_{SoC}. The variance of w is a tuning parameter for the filter. More details on Kalman filters can be found in e.g., [30, ch. 5]. Note that as the SoC cannot be directly measured it must be estimated. In addition, the terms "process noise" and "measurement noise" are misused to link the variables to commonly used terms for Kalman filters (e.g., the variance of v is the variance of a signal, not the variance of a measurement error).

Both $E[\text{SoC}]$ or σ_{SoC} can be controlled to fulfill (14). During the simulation study it was observed that when both were controlled the optimal solution was to reduce σ_{SoC} by decreasing the distance between $\underline{\tau}$ and $\bar{\tau}$. However, the desired performance is that $\underline{\tau}$ and $\bar{\tau}$ are used to control the temperature, while P_{MPC} is used to control the SoC. Therefore, σ_{SoC} is set to $\max[\sigma_{\text{SoC}}(\underline{\tau}, \bar{\tau})] = \sigma_{\text{SoC}}(\underline{\tau}_{\text{ref}}, \bar{\tau}_{\text{ref}})$. This gives a conservative performance of the SoC, and as long as $\text{SoC}_{\max} - \text{SoC}_{\min} \gg 2F^{-1}(1-\eta_{\text{SoC}})\sigma_{\text{SoC}}(\underline{\tau}_{\text{ref}}, \bar{\tau}_{\text{ref}})$ a feasible $E[\text{SoC}]$ exists.

IV. Model Predictive Control

To achieve the control objectives mentioned in Sec. II, an MPC is implemented. The decision variables of the controller are $\boldsymbol{\xi} = \begin{bmatrix}\underline{\tau} & \bar{\tau} & P_{\text{MPC}}\end{bmatrix}^\top$, with reference values $\boldsymbol{\xi}_{\text{ref}}$. Some slack variables are also used, to make sure that a feasible solution always exists, $\boldsymbol{s} = \begin{bmatrix}s^+_{\text{SoC}} & s^-_{\text{SoC}} & s_T\end{bmatrix}^\top$, with the reference $\boldsymbol{s}_{\text{ref}}$. s^+_{SoC} and s^-_{SoC} are slack variables for lower and upper SoC constraints, and s_T is the slack variable for the temperature constraint. The stage cost is:

$$\begin{aligned} l(\boldsymbol{\xi}, \boldsymbol{s}) =& h_1 \left(\frac{\underline{\tau}}{\underline{\tau}_{\text{ref}}} - 1\right)^2 + h_2 \left(\frac{\bar{\tau}_{\text{ref}}}{\bar{\tau}} - 1\right)^2 + h_3 P^2_{\text{MPC}} \\ &+ (\boldsymbol{s} - \boldsymbol{s}_{\text{ref}})^\top H_2 (\boldsymbol{s} - \boldsymbol{s}_{\text{ref}}) \end{aligned} \tag{21}$$

where h_1, h_2, and h_3 are positive constants and H_2 is a positive definite weight matrix. The chosen penalty function of $\underline{\tau}$ and $\bar{\tau}$ gives equal cost for doubling $\underline{\tau}$ as halving $\bar{\tau}$ from their reference. The costs of altering P_{MPC}, $\underline{\tau}$, and $\bar{\tau}$ are used as tuning parameters as these are the control inputs to the battery control system. This multi-objective cost function is equivalent to utopia tracking [31], with the exception of the neglected terminal constraint. Instead of terminal constraints, a long prediction horizon is used [32]. Other cost functions of the time constants were tested, such as:

$$l_2 = (\bar{\tau} - \bar{\tau}_{\text{ref}})^2 + (\underline{\tau} - \underline{\tau}_{\text{ref}})^2 \tag{22}$$

$$l_3 = \left(\frac{1}{\bar{\tau}} - \frac{1}{\bar{\tau}_{\text{ref}}}\right)^2 + \left(\frac{1}{\underline{\tau}} - \frac{1}{\underline{\tau}_{\text{ref}}}\right)^2 \tag{23}$$

$$l_4 = \ln^2\left(\frac{\bar{\tau}}{\bar{\tau}_{\text{ref}}}\right) + \ln^2\left(\frac{\underline{\tau}}{\underline{\tau}_{\text{ref}}}\right) \tag{24}$$

The l_2 and l_3 cost gives problems with scaling, as the MPC favors adjusting one of the variables, $\underline{\tau}$ and $\bar{\tau}$, respectively. Using a logarithmic cost, l_4, gives solutions quite close to those from using the chosen cost function. However, this cost suffers from numerical problems and ACADO was often unable to solve the optimization problem.

The optimization problem is:

$$\begin{aligned} \Psi^* = \underset{\Psi}{\operatorname{argmin}} & \sum_{k=0}^{N-1} l(\boldsymbol{\xi}(t_k), \boldsymbol{s}(t_k)) \\ \text{subject to } & (10), (15), \\ \text{SoC}_{\min} \le E[\text{SoC}(t_k)] &- F^{-1}(1-\eta_{\text{SoC}})\sigma_{\text{SoC}}(t_k) + s^-_{\text{SoC}}(t_k) \\ \text{SoC}_{\max} \ge E[\text{SoC}(t_k)] &+ F^{-1}(1-\eta_{\text{SoC}})\sigma_{\text{SoC}}(t_k) - s^+_{\text{SoC}}(t_k) \\ E[T(t_k)] &\le T_{\max} + s_T(t_k) \\ 0 &\le \boldsymbol{s}(t_k) \\ E[T(t_0)] &= T(t_0) \\ E[\text{SoC}(t_0)] &= \overline{\text{SoC}}(t_0) \end{aligned} \tag{25}$$

where

$$\Psi = \begin{bmatrix}\boldsymbol{\xi}(t_0) & \boldsymbol{s}(t_0) & \dots & \boldsymbol{\xi}(t_{N-1}) & \boldsymbol{s}(t_{N-1})\end{bmatrix}^\top$$

contains all the decision variables and Ψ^* is the optimal solution. Note that all state constraints are soft, by the use of slack variables. This means that the optimization problem is always feasible.

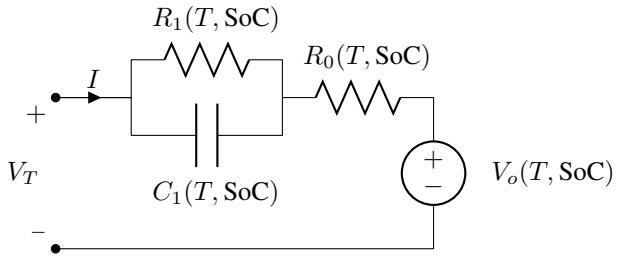

Fig. 3. Model of battery used in process plant with internal resistances, R_0 and R_1; capacitor, C_1; open circuit voltage, V_o, and output voltage and current V_T and I. All parameters are dependent on SoC and temperature. The model and parameters are adapted from [33].

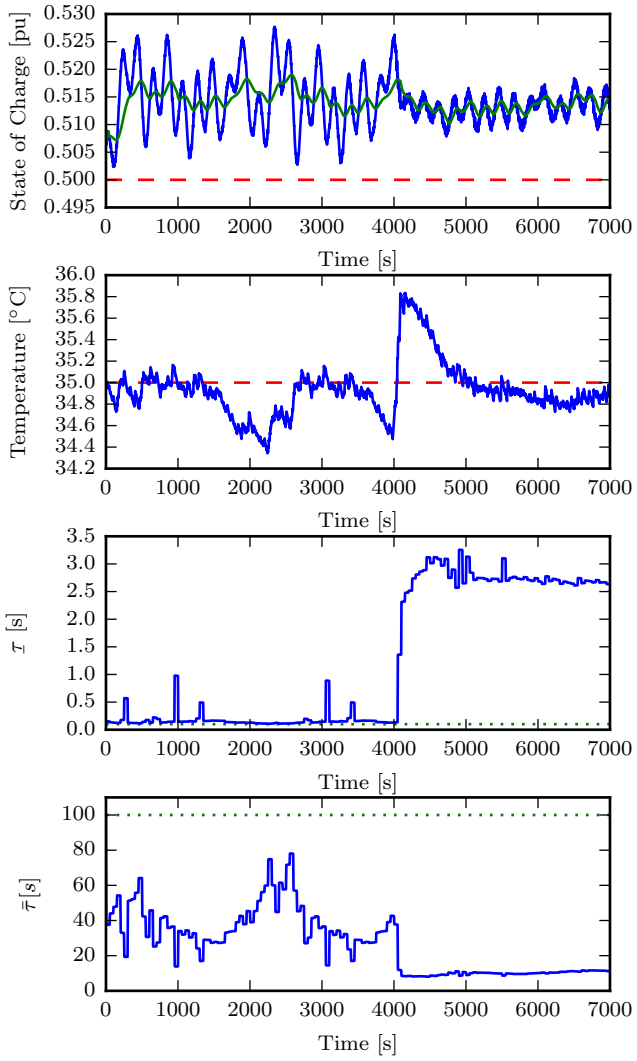

Fig. 4. Simulation described in Sec. V with Case 1. The red lines are the SoC and temperature constraints. The reference value for the time constant is the green dotted line. The solid green line is the estimated E[SoC] from the Kalman filter.

The first control input $\boldsymbol{\xi}^*(t_0)$ is applied. At each time instant (25) is re-optimized.

V. Simulation Study

In the simulation study, the controller is tested using a realistic model. The vessel is a supply vessel in dynamic positioning

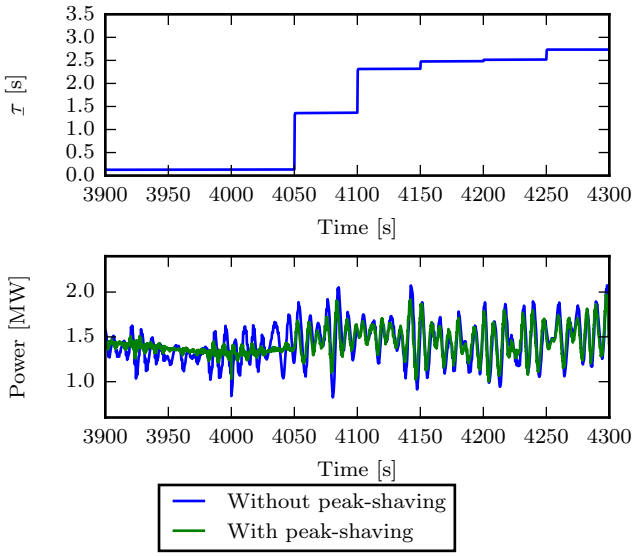

Fig. 5. Simulation with case plant as described in Sec. V with Case 1. At $t = 4000$ second the load variations increased. The time constant changed 50 seconds after the change of the load variations. This time lag is due to the time lag of the estimated power spectral density; however, the MPC reacts to an increased battery temperature.

operation. The power load is generated by the model presented in [34]. The significant wave height is 4 meters. The vessel has five thrusters, two 1.5 MW, two 2.7 MW, and one 850 kW thruster. Four diesel generator sets are used to produce electric power, two 2.2 MW and two 3.3 MW generators. A load proportional to the heave velocity is included to simulate a heave compensator. These loads are not Gaussian, as assumed earlier for the chance constraints. The battery model presented in [33] is used as the process plant model for the simulations (Fig. 3). This model includes an RC-circuit in addition to the internal resistance. Additionally, the resistance, capacitance, and internal voltage are dependent on the temperature and state of charge. The parameters are given for the high power lithium cell (LiNi-CoMnO$_2$ cathode and graphite-based anode), 31Ah Kokam SLPB 78216216H. The parameters of the control model in the MPC are found by using the parameters of the process plant model at the minimum state of charge (50%) and maximum temperature (35 °C). The power spectral density of P_{load} is estimated using a moving window of the last 1000 seconds of the measurements. ACADO [35] is used to implement the controller and the simulations are performed in MATLAB/SIMULINK. The MPC is reoptimized every 50 seconds and the horizon length is set to 10 samples (500 seconds), which is long enough to include most cooling dynamics. The Kalman filter is updated every 10 seconds, with $\sigma_w^2 = 4 \times 10^{-8}$. It is tuned (by setting σ_w^2) to give a good balance between the phase lag of the estimation and the size of the ripples from the SoC variations. The length of the horizon is chosen to be long enough to capture some cooling effects. The update time is chosen to be small enough to avoid a large temperature increase after a sudden change in the characteristics of the load. The remaining parameters used in the simulation are given in Tab. I. ACADO uses less

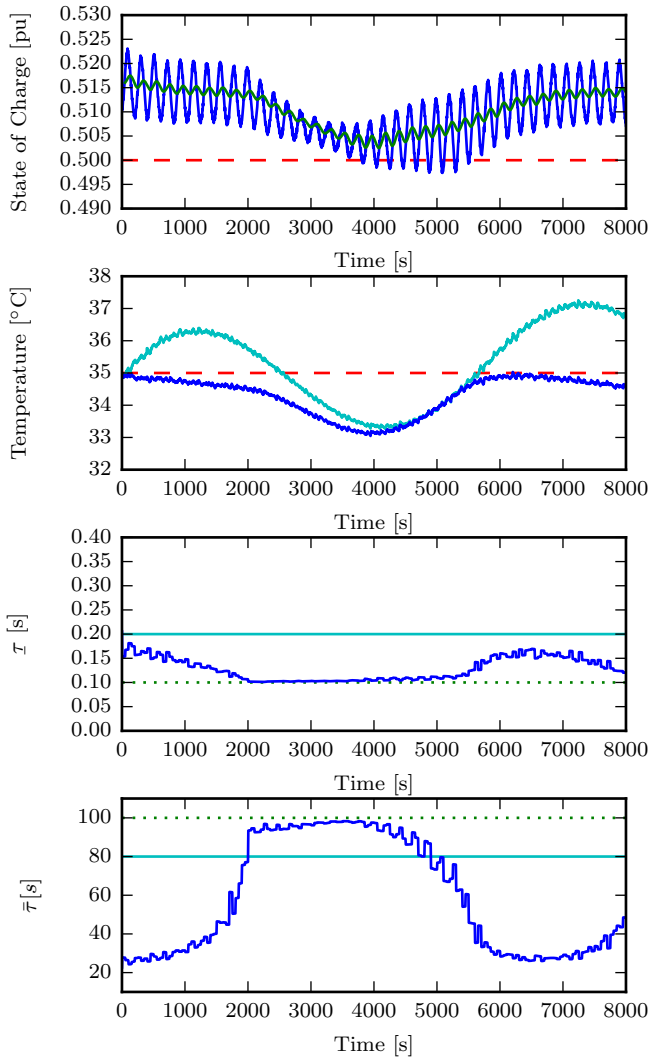

Fig. 6. Simulation described in Sec. V with Case 2. The red lines are the SoC and temperature constraints. The reference value for the time constant is the green dotted line. The solid green line is the estimated E[SoC] from the Kalman filter. The results with the controller with fixed time constant are shown in cyan. The SoC is not shown for this controller, since it was not controlled.

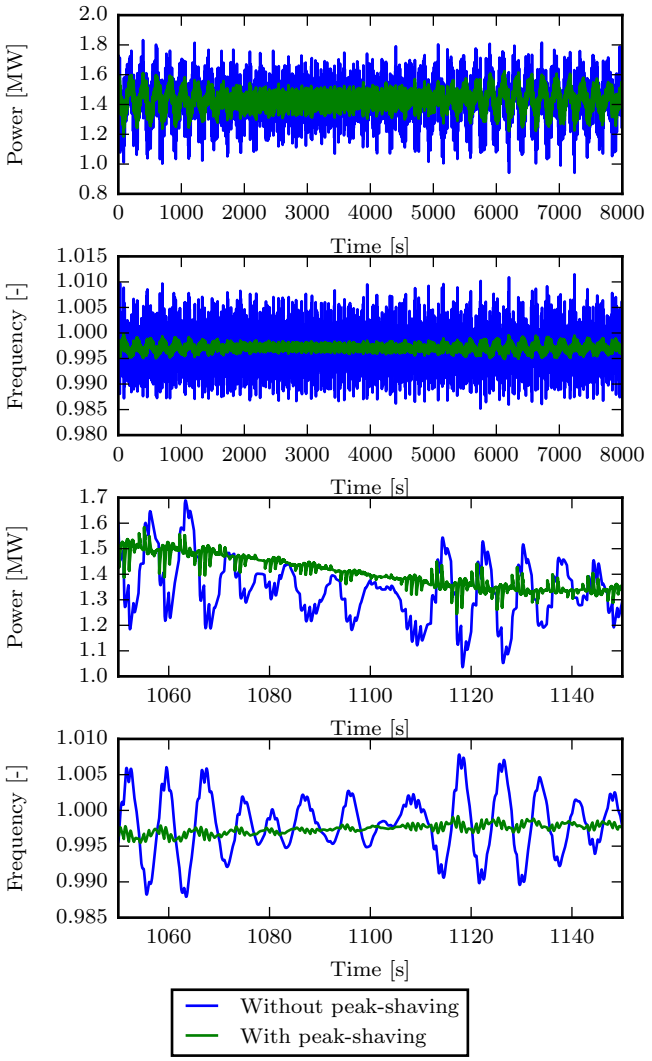

Fig. 7. Simulation described in Sec. V with Case 2. The resulting electrical frequency and power generated by the generators, with (green) and without (blue) power smoothing. The two lower plots are zoom-ins of the two upper plots.

than 1 second per update using a 3.5 GHz Intel® Xeon™ E3 processor. Hence, the algorithm is able to run in real-time on a less powerful industrial controller, including running power spectral density estimation, the Kalman filter, and the MPC.

Two load cases are simulated:

Case 1: A data series of 3000 seconds is generated and repeated three times. This is performed to illustrate the steady-state performance of the controller. The standard deviation of the heave compensator is 50 kW the first 4000 seconds; thereafter, it is increased to 200 kW. The average total load (P_{load}) is 1.43 MW and its standard deviation is 134 kW during the first 4000 seconds and 253 kW thereafter. This case is used to illustrate the performance of the power smoothing algorithm when the characteristic suddenly changes, such as when a new operation is started. Results are shown in Figs. 4 and 5.

Case 2: A single time series is used to illustrate the adaptiveness when the variance of the power consumption is slowly changing. The standard deviation of the heave compensator's power consumption is 50 kW. The present controller is compared with a power smoothing controller where $\underline{\tau} = 0.2$ seconds and $\bar{\tau} = 80$ seconds. Results are shown in Figs. 6 and 7.

Results from the simulation with Case 1 are shown in Fig. 4. It is clear that the time average of the SoC is controlled to a level above SoC_{min}. The Kalman filter gives a good estimate of the $E[\text{SoC}]$ when the SoC variations are large, as most of the peak variations are filtered out and the estimate is close to the middle between the peaks. However, the Kalman filter is not able to filter out small variations after 4000 seconds and the estimate stays closer to SoC. We can tolerate this as the SoC variations are small. The variance of the temperature is also small, it is therefore reasonable to constrain the expected temperature and not use probabilistic constraints. After 4000 seconds, the temperature increases rapidly due to the increased variation in the power demand. However,

the controller takes action at the first update of the MPC after the battery temperature starts to increase. Details of the transition of the load at 4000 seconds in Case 1 are shown in Fig. 5. Most of the load fluctuations are canceled out until 4050 seconds. At this instant, the time constants are changed to reduce the increased heat created during the previous interval. The band-pass filter is then narrowed to time constants of 3 and 7 seconds, which are typically difficult time scales for diesel engines. Most of the large power variations have periods larger than 10 seconds, this means that they are not canceled. Therefore, power smoothing will be reduced when the power variations are large, as the battery is not able to cancel the variations without overheating. However, the battery still cancels out the most critical power variations. The temperature constraint is violated multiple times during the first 1500 seconds. This occurs because the mean temperature is constrained, while the temperature fluctuates due to the power variations. The violations are smaller than 0.1 °C. A temperature safety margin should be included to handle the small violations caused by temperature fluctuation and rapid temperature increases due to the change in the load characteristics.

Results from the simulation of Case 2 are shown in Figs. 6 and 7. During this simulation the variance of P_{load} slowly changes. The time constants of the band-pass filter change dynamically so that it is wide when the battery temperature is low, and narrow when it is high. It maintains the temperature below the temperature limits when the variance increases. In contrast, the fixed time constant approach gives too high temperatures. The filter does not utilize the full potential of the power smoothing capability when the temperature is low. This approach would require the filter to be frequently tuned manually or have a very conservative tuning. Safety protection in the battery will temporarily disconnect it if the temperature gets too high, which typically occurs when the variations are at their largest and power smoothing is most needed. Between 3500 and 4500 seconds, when the fluctuations increase again, the SoC constraint (8) is violated 11.5% of the time. This is mainly due to the lag in the estimation of the power spectral density. It may also occur due to the approximation of the load being Gaussian, which is not true for the simulated load. The fulfillment of the constraint can be increased by improving the estimate of the statistical properties of the load variations, e.g., better prediction of the variance or more correct probability distribution. Other types of chance constraints were tested such as cVaR [25], which is able to handle nonlinear models, but increased the computational demand. However, we did not see any significant reduction in the violation of the chance constraints. This may be because the errors in the estimate of future statistical properties of the load variations are typically much larger than the linearization errors. The Kalman filter is able to filter out most of the SoC variations. However, some small ripples are left and a small phase lag between the mean SoC and the estimated mean SoC is visible. A reduction of ripples gives an increase in the phase lag; the filter is therefore tuned to give a good compromise between ripples and phase lag.

Simulation results with and without power smoothing are shown in Fig. 7, which shows the power demand on the generator sets and the electrical frequency. It shows that power smoothing reduces the power and frequency variations during the entire simulation, although more variations are canceled when the band-pass filter is wide. The low-frequency variation in the electrical frequency is much smaller than the power variations during the first 1000 seconds, and these variations are slow enough to be handled by the diesel engine. The remaining low frequency variation in the electric frequency is a result of frequency droop in the governor for load sharing control. The lower two plots show a zoom-in of the upper two and it is clear that most of the remaining variations in the frequency are high frequency variations, which are handled by the inertia of the generator set. This reduction of electrical frequency variations makes it easier to synchronize a new generator set to the grid, and reduced power variations also decrease wear and tear on the generator set and possibly lower fuel consumption.

TABLE I
PARAMETERS USED IN SIMULATION. PARAMETERS FOR THE PROCESS PLANT BATTERY MODEL CAN BE FOUND IN [33].

Parameter	Value
$\underline{\tau}_{\text{ref}}$	0.1 s
$\bar{\tau}_{\text{ref}}$	100 s
V_o	3.71 V
Q_{nominal}	27.6 Ah
R_i	0.0096 Ω
c	810 $\frac{J}{K}$
$\frac{hA}{c}$	1591 s
n_{cells}	1323
$T_{\max}$	35 °C
$\text{SoC}_{\min}$	0.50
$\text{SoC}_{\max}$	0.90
η_{SoC}	5%
$h_1 = h_2$	1
h_3	0.1
$\boldsymbol{s}_{\text{ref}}$	$\begin{bmatrix}-10 & -10 & -10\end{bmatrix}^\top$
H_2	$\begin{bmatrix}100 & 0 & 0\\ 0 & 100 & 0\\ 0 & 0 & 100\end{bmatrix}$

VI. CONCLUSION

In this paper it is demonstrated how power spectral density can be used to estimate expected values, variance in the state of charge, and the expected temperatures of a battery. This is used in the optimization problem of the MPC. A power smoothing example is used to demonstrate the control scheme. The MPC sets the time constants of a band-pass filter that controls the power smoothing performed by the battery. The controller's objective is to maintain the battery temperature below a maximum and the state of charge within a desired range. It is shown that controller achieves its control objectives by controlling the temperature and state of charge close to the constraints. However, the constraints are violated after a sudden change in the load characteristics. The power smoothing algorithm cancels out the variations that are most difficult to handle by the diesel engines, giving less variation in the electrical frequency.

APPENDIX

A. Mathematical Preliminaries

Given a linear system with random input x, transfer function $H(j\omega)$, and output y. The periodogram of x is $p_{xx}(\omega)$. For such a system, the periodogram of y is

$$p_{yy}(\omega) = p_{xx}(\omega)|H(j\omega)|^2. \tag{26}$$

The variance and power of the signal are given as

$$\sigma_x^2 = \int_0^\infty p_{xx}(\omega)\,\mathrm{d}\omega. \tag{27}$$

Given a normal distributed variable X, with the mean and variance $\bar{x}$ and σ^2. The probability constraint

$$\text{Prob}(X > x_c) \geq 1 - \eta$$

is equivalent to

$$x_c < \bar{x} - F^{-1}(1-\eta)\sigma \tag{28}$$

where η is the probability threshold, and $F^{-1}(\cdot)$ is the inverse probability distribution of standard normal distribution.

REFERENCES

[1] A. Veksler, T. A. Johansen, and R. Skjetne, "Transient power control in dynamic positioning - governor feedforward and dynamic thrust allocation," in *IFAC conference on manoeuvring and control of marine craft*, 2012.

[2] E. Mathiesen, B. Realfsen, and M. Breivik, "Methods for reducing frequency and voltage variations on DP vessels," in *MTS Dynamic Positioning Conference*, 2012.

[3] D. Radan, A. J. Sørensen, A. K. Ådnanes, and T. A. Johansen, "Reducing power load fluctuations on ships using power redistribution control," *Marine Technology*, vol. 45, no. 3, pp. 162–174, 2008.

[4] T. A. Johansen, T. I. Bø, E. Mathiesen, A. Veksler, and A. J. Sørensen, "Dynamic positioning system as dynamic energy storage on diesel-electric ships," *IEEE Transactions on Power Systems*, vol. 29, no. 6, pp. 3086–3091, Nov 2014.

[5] X. Shi, Y. Wei, J. Ning, M. Fu, and D. Zhao, "Optimizing adaptive thrust allocation based on group biasing method for ship dynamic positioning," in *IEEE International Conference on Automation and Logistics (ICAL)*, Aug 2011, pp. 394–398.

[6] Eidsvik, "Viking Queen installation of energy storage system," May 2015, accessed: 2015-08-27. [Online]. Available: www.eidesvik.no/news-archive/viking-queen-installation-of-energy-storage-system-article645-299.html

[7] F. Martini, "First electrical car ferry in the world in operation in Norway now," in *Siemens, Pictures of the Future*, May 2015.

[8] B. M. Huhman and D. A. Wetz, "Progress in the Development of a Battery-based Pulsed Power System," in *IEEE Electric Ship Technology Symposium (ESTS)*, 2015, pp. 441–445.

[9] S. Kuznetsov, "Large Scale Energy Storage Module for Surface Combatants : Transmission and System Transient Characteristics," in *IEEE Electric Ship Technology Symposium (ESTS)*, 2015, pp. 167–172.

[10] S.-Y. Kim, S. Choe, S. Ko, and S.-K. Sul, "A naval integrated power system with a battery energy storage system: Fuel efficiency, reliability, and quality of power." *IEEE Electrification Magazine*, vol. 3, no. 2, pp. 22–33, June 2015.

[11] J. Hou, J. Sun, and H. Hofmann, "Mitigating power fluctuations in electrical ship propulsion using model predictive control with hybrid energy storage system," in *American Control Conference (ACC)*, June 2014, pp. 4366–4371.

[12] Y. Tang and A. Khaligh, "On the feasibility of hybrid battery/ultracapacitor energy storage systems for next generation shipboard power systems," in *IEEE Vehicle Power and Propulsion Conference*, Sept 2010, pp. 1–6.

[13] J. Hou, J. Sun, and H. Hofmann, "Interaction analysis and integrated control of hybrid energy storage and generator control system for electric ship propulsion," in *American Control Conference (ACC)*, July 2015, pp. 4988–4993.

[14] D. Hermance and S. Sasaki, "Hybrid electric vehicles take to the streets," *IEEE Spectrum*, vol. 35, no. 11, pp. 48–52, Nov 1998.

[15] S. J. Moura, H. K. Fathy, D. S. Callaway, and J. L. Stein, "A stochastic optimal control approach for power management in plug-in hybrid electric vehicles," *IEEE Transactions on Control Systems Technology*, vol. 19, no. 3, pp. 545–555, May 2011.

[16] C.-C. Lin, H. Peng, J. W. Grizzle, and J.-M. Kang, "Power management strategy for a parallel hybrid electric truck," *IEEE Transactions on Control Systems Technology*, vol. 11, no. 6, pp. 839–849, Nov 2003.

[17] V. H. Johnson, K. B. Wipke, and D. J. Rausen, "HEV control strategy for real-time optimization of fuel economy and emissions," SAE Technical Paper, Tech. Rep., 2000.

[18] J. Zeng, B. Zhang, C. Mao, and Y. Wang, "Use of battery energy storage system to improve the power quality and stability of wind farms," in *International Conference on Power System Technology (PowerCon)*, Oct 2006, pp. 1–6.

[19] R. Sebastián and J. Quesada, "Distributed control system for frequency control in a isolated wind system," *Renewable Energy*, vol. 31, no. 3, pp. 285 – 305, 2006.

[20] D. Kottick, M. Blau, and D. Edelstein, "Battery energy storage for frequency regulation in an island power system," *IEEE Transactions on Energy Conversion*, vol. 8, no. 3, pp. 455–459, Sep 1993.

[21] P. Stone, D. F. Opila, H. Park, J. Sun, S. Pekarek, R. DeCarlo, E. Westervelt, J. Brooks, and G. Seenumani, "Shipboard power management using constrained nonlinear model predictive control," in *IEEE Electric Ship Technologies Symposium (ESTS)*, June 2015, pp. 1–7.

[22] H. Park, J. Sun, S. Pekarek, P. Stone, D. Opila, R. Meyer, I. Kolmanovsky, and R. DeCarlo, "Real-time model predictive control for shipboard power management using the IPA-SQP approach," *IEEE Transactions on Control Systems Technology*, vol. PP, no. 99, pp. 1–1, 2015.

[23] T. I. Bø and T. A. Johansen, "Scenario-based fault-tolerant model predictive control for diesel-electric marine power plant," in *OCEANS - Bergen, 2013 MTS/IEEE*, June 2013, pp. 1–5.

[24] F. Oldewurtel, A. Parisio, C. N. Jones, M. Morari, D. Gyalistras, M. Gwerder, V. Stauch, B. Lehmann, and K. Wirth, "Energy efficient building climate control using stochastic model predictive control and weather predictions," in *American Control Conference (ACC)*, June 2010, pp. 5100–5105.

[25] K. G. Hanssen, B. Foss, and A. Teixeira, "Production optimization under uncertainty with constraint handling," in *2nd IFAC Workshop on Automatic Control in Offshore Oil and Gas Production*, May 2015, pp. 62–67.

[26] J. Matusko and F. Borrelli, "Scenario-based approach to stochastic linear predictive control," in *IEEE 51st Annual Conference on Decision and Control (CDC)*, Dec 2012, pp. 5194–5199.

[27] S. Piller, M. Perrin, and A. Jossen, "Methods for state-of-charge determination and their applications," *Journal of Power Sources*, vol. 96, no. 1, pp. 113 – 120, 2001.

[28] G. L. Plett, "Extended kalman filtering for battery management systems of LiPB-based HEV battery packs: Part 3. state and parameter estimation," *Journal of Power Sources*, vol. 134, no. 2, pp. 277 – 292, 2004.

[29] I.-S. Kim, "Nonlinear state of charge estimator for hybrid electric vehicle battery," *IEEE Transactions on Power Electronics*, vol. 23, no. 4, pp. 2027–2034, July 2008.

[30] R. G. Brown and P. Y. Hwang, *Introduction to Random Signals and Applied Kalman Filtering*, 3rd ed. Wiley, 1997.

[31] V. M. Zavala and A. Flores-Tlacuahuac, "Stability of multiobjective predictive control: A utopia-tracking approach," *Automatica*, vol. 48, no. 10, pp. 2627 – 2632, 2012.

[32] L. Grüne and J. Pannek, *Nonlinear Model Predictive Control: Theory and Algorithms*. London: Springer London, 2011, ch. Stability and Suboptimality Without Stabilizing Constraints, pp. 113–163.

[33] T. Huria, M. Ceraolo, J. Gazzarri, and R. Jackey, "High fidelity electrical model with thermal dependence for characterization and simulation of high power lithium battery cells," in *IEEE International Electric Vehicle Conference (IEVC)*, March 2012, pp. 1–8.

[34] T. I. Bø, A. R. Dahl, T. A. Johansen, E. Mathiesen, M. R. Miyazaki, E. Pedersen, R. Skjetne, A. J. Sørensen, L. Thorat, and K. K. Yum, "Marine vessel and power plant system simulator," *IEEE Access*, vol. 3, pp. 2065–2079, 2015.

[35] B. Houska, H. J. Ferreau, and M. Diehl, "ACADO toolkit – an open source framework for automatic control and dynamic optimization," *Optimal Control Applications and Methods*, vol. 32, no. 3, pp. 298–312, 2011.